Available online at www.sciencedirect.com
ScienceDirect
International Journal of Heat and Mass Transfer 50 (2007) 3366–3375
International Journal of HEAT and MASS TRANSFER
www.elsevier.com/locate/ijhmt

Experimental investigation on the heat transfer of an impinging inverse diffusion flame

T.K. Ng *, C.W. Leung, C.S. Cheung

Department of Mechanical Engineering, The Hong Kong Polytechnic University, Hong Kong, China

Received 21 August 2006; received in revised form 22 January 2007
Available online 6 April 2007

Abstract

This paper presents the results of an experimental study on the heat transfer characteristics of an inverse diffusion flame (IDF) impinging vertically upwards on a horizontal copper plate. The IDF burner used in the experiment has a central air jet surrounded circumferentially by 12 outer fuel jets. The heat flux at the stagnation point and the radial distribution of heat flux were measured with a heat flux sensor. The effects of Reynolds number, overall equivalence ratio, and nozzle-to-plate distance on the heat flux were investigated. The area-averaged heat flux and the heat transfer efficiency were calculated from the radial heat flux within a radial distance of 50 mm from the stagnation point of the flame, for air jet Reynolds number (Re_{air}) of 2000, 2500 and 3000, for overall equivalence ratios (Φ) of 0.8–1.8, at normalized nozzle-to-plate distances (H/d_{IDF}) between 4 and 10. Similar experiments were carried out on a circular premixed impinging flame for comparison.

It was found that, for the impinging IDF, for Φ of 1.2 or higher, the area-averaged heat flux increased as the Re_{air} or Φ was increased while the heat transfer efficiency decreased when these two parameters increased. Thus for the IDF, the maximum heat transfer efficiency occurred at $Re_{air} = 2000$ and $\Phi = 1.2$. At lower Φ, the heat transfer efficiency could increase when Φ was decreased. For the range of H/d_{IDF} investigated, there was certain variation in the heat transfer efficiency with H/d_{IDF}. The heat transfer efficiency of the premixed flame has a peak value at $\Phi = 1.0$ at $H/d_P = 2$ and decreases at higher Φ and higher H/d_P. The IDF could have comparable or even higher heat transfer efficiency than a premixed flame.

1. Introduction

Direct flame impingement heat transfer has many industrial and domestic applications. The heat transfer is affected by factors such as the nature of the flame, the Reynolds number of the fluid flow, the fuelling rate, and the distance between the nozzle of the burner and the heating object. Due to the complexity of the problem, there is continued effort in investigating the heat transfer characteristics of impinging flames.

A comprehensive review of flame impingement heat transfer has been given by Chander and Ray [1]. The heat transfer characteristics of the circular and slot premixed impinging flame jets have been investigated by several investigators including Dong et al. [2], Kwok et al. [3], Huang et al. [4], Tuttle et al. [5] and Zhao et al. [6]. They investigated the effect of Reynolds number of the flow, equivalence ratio of the air fuel mixture, the nozzle-to-plate distance, as well as the characteristics of the impingement surface and the flame, on the heat transfer. Dong et al. [7,8] and Kwok et al. [9] also investigated the heat transfer of multiple impinging flame jets.

One important aspect of heat transfer is the efficiency of the heat transfer process which has been mentioned only in a limited number of literatures. Hou and Ko [10] investigated the effects of heating height on the appearance, temperature field and efficiency of a premixed impinging laminar flame jet. They found that the maximum efficiency occurred when the heating height was slightly lower than the tip of the inner rich premixed flame. Mizuno et al.

* Corresponding author.
E-mail address: selina.ng@polyu.edu.hk (T.K. Ng).

0017-9310/$ - see front matter © 2007 Elsevier Ltd. All rights reserved.
doi:10.1016/j.ijheatmasstransfer.2007.01.046

Nomenclature

A	integration area (m^2)
H	distance between the nozzle and the impingement plate (mm)
D	effective diameter (mm)
H/d	nozzle-to-plate distance
IDF	inverse diffusion flame
LHV	low heating value of gas fuel (kJ/kg)
LPG	liquefied petroleum gas
$\dot{Q}$	volumetric flow rate (m^3/s)
$\dot{q}$	heat flux density (W/m^2)
$\bar{q}$	area-averaged heat flux (W/m^2)
Re	Reynolds number
r	radial distance from stagnation point (mm)
η	heat transfer efficiency
Φ	overall equivalence ratio
ρ	density (kg/m^3)

Subscripts

air	the compressed air
f	Fuel
IDF	inverse diffusion flame
mix	mixture of air and fuel
P	premixed flame

[11] investigated the heat transfer efficiency of an impinging premixed flame, and concluded that the heat transfer increased with increasing heat input but the thermal efficiency decreased at the same time. Similar results were shown by Baudal and Gebhart [12] who investigated an oxygen-enhanced premixed flame. They reported that the thermal efficiency decreased with firing rate and the heating height, but increased with the oxidizer purity. Therefore, in application, high firing rates can enhance productivity but reduce the thermal efficiency.

Most of the former investigations on impinging flames are concerned with premixed flames. However, there is strong limitations on the fuelling rate and the equivalence ratio of the premixed air fuel mixture in order to avoid flame lifting or soot formation. Sze et al. [13] investigated the heat transfer characteristics of an inverse diffusion flame (IDF) for impingement heating. They found that the IDF, compared with a premixed flame, has lower peak heat flux but could provide higher fuelling rate and more uniform heating around the stagnation point.

The basic characteristics of IDF have been investigated and reported in [14–18]. The flames investigated in [14–18] were coaxial flames with an inner air jet and an outer fuel jet. The flames formed consist of an inner premixed bluish combustion zone overlapped by an outer yellowish diffusion combustion zone. The IDF produces much less soot than the normal diffusion flames with the same fuelling rate. The IDF investigated by Sze et al. [13,19] has a central air jet surrounded by circumferentially arranged fuel jets. They found that the circumferentially arranged fuel ports enable better air fuel mixing than the coaxial jets [19].

This paper aims to study the heat transfer characteristics of an impinging IDF, with circumferentially arranged fuel ports. A heat-transfer-efficiency is defined for evaluation of the efficiency of the burner in transferring energy from the fuel to the impingement plate. At the same time, the heat transfer characteristics and the heat transfer efficiency of a premixed flame jet are also investigated for comparison.

2. Experimental work and method of analysis

Two burners were used in this study, namely an IDF and a circular premixed burner. The IDF burner used in this investigation is shown in Fig. 1. It is similar to the one used in [13,19]. There are 12 outer fuel jets of 2.4 mm diameter each surrounding a central air jet of 6 mm diameter. The centre-to-centre distance between the air jet and the fuel jets is 8 mm in the present study but 11.5 mm in [13,19]. The circular premixed burner has a nozzle of 9.3 mm inner diameter. The effective diameter of the IDF (d_{IDF}) is defined as the diameter of the air jet, 6 mm, and that of the premixed flame (d_P) is referred to the nozzle exit diameter, 9.3 mm. Thus, the two burners have almost the same total exit areas for the air and fuel.

The experimental system is shown schematically in Fig. 1. LPG consisting of 70% butane and 30% propane is used in the experiments. It is the standard composition of LPG available in Hong Kong. LPG and compressed air were metered by rotameters before entering the burners. The three-dimensional positioner enabled adjustment of the burner position relative to the impingement surface.

The target plate was a water-cooled copper plate with a surface area of $500 \times 500\ mm^2$ and 8 mm thick [3]. It was evenly cooled on the backside by a cooling water jacket. The temperature of cooling water was maintained automatically at 38 °C by a thermostat to avoid condensation. At the plate center, a heat flux sensor was attached to measure the heat flux, which was a small ceramic heat flux transducer (Vatell Corporation, Model HFM-6D/H) with an effective sensing area of $2 \times 2\ mm^2$. It was mounted with the impingement plate according to the manufacturer's specifications with a ± 0.01 mm dimensional tolerance to ensure that the sensor and the plate surface were in the same alignment. The standard coating for the face of the sensor is zynolyte, which is a high temperature black coating with a 0.94 emissivity. It was recommended that applications involving radiative heat transfer use a coated transducer because the absorption properties are better.

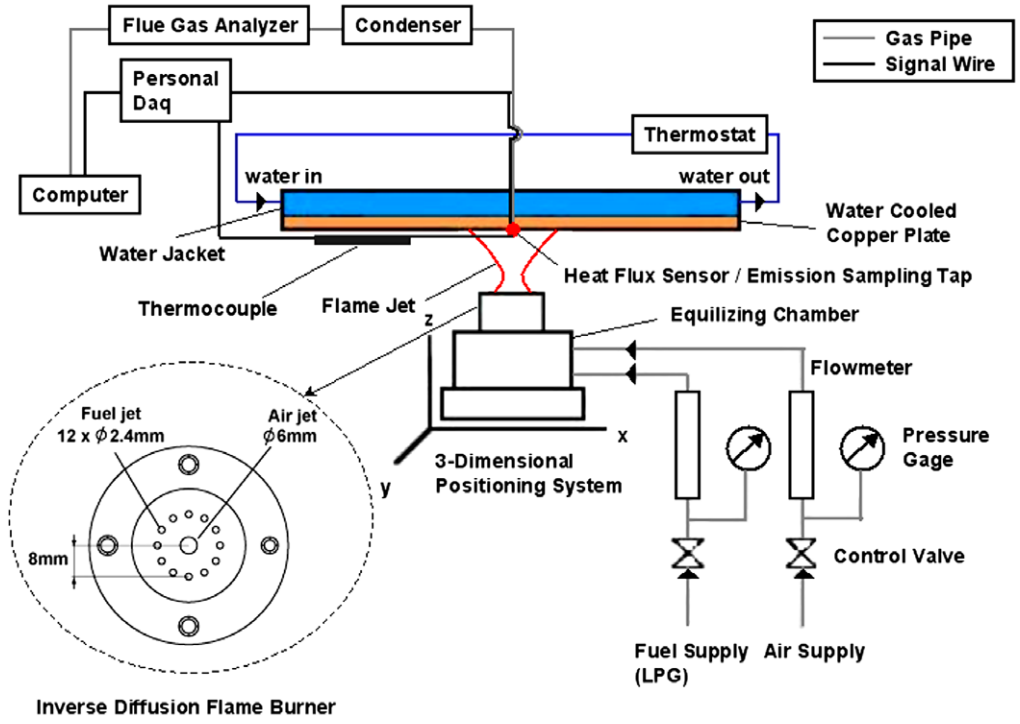

Fig. 1. Schematic of the experimental set-up.

The sensor came with a NIST traceable calibration certificate by the manufacturer that provided all of the information necessary to convert the signals from the sensor to their heat flux values and the accuracy was ±3%. The voltage signals received by the transducer were amplified by a low noise, wide-band differential signal conditioning amplifier with an accuracy of ±1.5%.

In this study, the heat flux reported was recorded only after a steady state had been achieved and was a time-averaged value obtained consecutively in 2 min at a sampling rate of 8 data per second. An uncertainty analysis was carried out with the method proposed by Kline and McClintock [20]. Using a 95% confidence level, the maximum and minimum uncertainties in the presented local heat flux were 14% and 0.2%.

Experiments were performed using the IDF at three air flow rates corresponding to Re_{air} of 2000, 2500 and 3000, with overall equivalence ratios (Φ) varying from 0.8 to 1.8. In this paper, for the IDF, Re_{air} refers to the Reynolds number of the air jet based on the air jet velocity and the air jet diameter. For an IDF, the air and fuel are not premixed. Hence, it does not have a well defined equivalence ratio for the air fuel mixture. To reflect the fueling rate, an overall equivalence ratio is used. The overall equivalence ratio is defined as the equivalence ratio of the mixture if the air from the air jet and the fuel from the fuel jets are mixed together. Thus, the higher the overall equivalence ratio, the higher the fueling rate, for a certain Re_{air}. For each operating condition, the stagnation point heat flux was measured for nozzle-to-plate distance (H) varying from $H = 12$ mm to 96 mm, corresponding to $H/d_{IDF} =$ 2–16, to identify the range of nozzle-to-plate distance of interest. Subsequently, at $H/d_{IDF} = 5$, 6, 7 and 8, the radial heat flux distribution on the impingement plate was measured from the centre to a radial distance of 50 mm for different combinations of Re_{air} and Φ. For $Re_{air} = 2000$, the radial heat flux distribution measurement was extended to cover the range of H/d_{IDF} from 4 to 10. Table 1 shows the experimental conditions for the IDF.

Table 1
Experimental conditions for the IDF

Re_{air}	Φ	Air jet velocity (m/s)	Fuel jet velocity (m/s)	Air flow rate ($\times 10^{-4}$ m^3/s)	Total Fuel flow rate ($\times 10^{-6}$m^3/s)
2000	0.8	5.08	0.07	1.44	3.71
2000	1	5.08	0.09	1.44	4.63
2000	1.2	5.08	0.10	1.44	5.56
2000	1.4	5.08	0.12	1.44	6.49
2000	1.6	5.08	0.14	1.44	7.41
2000	1.8	5.08	0.15	1.44	8.34
2500	0.8	6.35	0.09	1.79	4.63
2500	1	6.35	0.11	1.79	5.79
2500	1.2	6.35	0.13	1.79	6.95
2500	1.4	6.35	0.15	1.79	8.11
2500	1.6	6.35	0.17	1.79	9.26
2500	1.8	6.35	0.19	1.79	10.42
3000	0.8	7.61	0.10	2.15	5.56
3000	1	7.61	0.13	2.15	6.95
3000	1.2	7.61	0.15	2.15	8.34
3000	1.4	7.61	0.18	2.15	9.73
3000	1.6	7.61	0.21	2.15	11.11
3000	1.8	7.61	0.23	2.15	12.51

Experiments were then performed for the premixed flame. The air and fuel flow rates used were the same as those of the IDF at $Re_{air} = 2000$ with $\Phi = 1.0$ and $\Phi = 1.2$. The radial heat flux distribution was measured for $H/d_P = 1.5$–4, with the same radial distance of 50 mm. In this study, the two burners are compared under the same fuel flow rate which has stronger influence on the heat flux distribution. Since the two burners have almost the same total exit areas, for the same fuel flow rate and air flow rate, the two burners have different exit velocities and hence the Re_{IDF} and Re_{mix} are also different.

Based on the radial heat fluxes, the area-averaged heat flux and the heat transfer efficiency can be calculated using Eqs. (1) and (2) respectively,

$$\bar{\dot{q}} = \frac{\int\int^{A} \dot{q}\,\mathrm{d}A}{A} = \frac{2\pi\int_0^R \dot{q} r\,\mathrm{d}r}{\pi R^2} \tag{1}$$

$$\eta\ (\%) = \frac{\text{Output}}{\text{Input}} \times 100\% = \frac{\bar{\dot{q}} \times A}{\dot{Q}_f \rho_f \mathrm{LHV}} \times 100\% \tag{2}$$

The area-averaged heat flux is obtained by integrating the local radial distribution of heat fluxes within a circular zone of 50 mm radius at the central region of the impingement plate. The heat flux is usually higher in the stagnation region and drops rapidly in the wall jet region. Thus, the average heat transfer decreases if the integration area is increased significantly into the wall jet region. Mahmood [21] has the same conclusion that the average heat transfer was greatly dependent on the integration area. Eq. (2) shows that the heat transfer efficiency is calculated as the percentage of energy from the fuel absorbed by the plate. However, the efficiency is dependent on the value of the total heat flux integrated from the radial distribution, that is, it increases with increasing integration area. In different cases, the radial heat flux decays at different rates. Thus, a common area based on a radius of 50 mm is chosen for both area-averaged heat flux and heat transfer efficiency calculation for all operating conditions. The radial distance of 50 mm is chosen because in most cases, the radial heat flux would have decayed by more than 90% over this radial distance. Tuttle et al. [5] defined a heating value fraction and investigated the variation of heating value with the radius of integration for different operating conditions. The concept is similar to that shown in Eq. (2) except that it is integrated to various radial positions. Their results also show an increase of the heating value fraction with increasing radius of integration.

3. Experimental results

3.1. Flame shapes

The upper part of Fig. 2 shows the open IDF flames for $Re_{air} = 2000$ and $\Phi = 0.8$–2.4. In each case, the fuel jets are attracted towards the air jet, creating a neck separating the flame into two parts, a base and an elongated main flame. The fuel jets mixed with the air to form a premixed air fuel mixture. Thus, for each flame, there is an intense bluish premixed combustion zone overlapping an inner cooler zone where air is exiting from the air jet; and overlapped by an outer yellowish diffusion combustion zone at high level of overall equivalence ratios. Fig. 2 shows that the open flame is mainly blue in colour up to $\Phi = 1.6$ while there is increasing diffusion combustion as Φ is increased. At a constant Re_{air} value, an increase in Φ indicates that more fuel is burned. Consequently there is an increase in flame length.

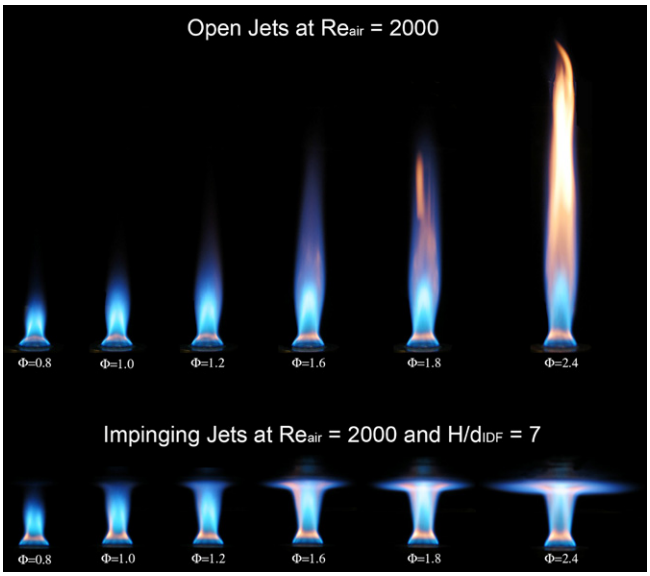

Fig. 2. Comparison of flame shapes of open and impinging IDF.

At a constant value of Φ, an increase in Re_{air} means that both air and fuel flow rates increase. The flame shapes are similar at $Re_{air} = 2500$ and 3000 except that due to the stronger air jet flow, there is stronger mixing between the air and the fuel, resulting in more intense combustion. Thus the corresponding flames are longer, due to the increased fuel flow rate, and with less diffusion combustion, due to the enhanced mixing.

The lower part of Fig. 2 shows the corresponding flames with the impingement plate located at a distance of 42 mm above the nozzle of the IDF, corresponding to H/d_{IDF} of 7. For $\Phi = 0.8$, the visible flame is not yet touching the plate. For $\Phi = 1.0$–1.8, the visible flame is touching the plate, and the tip of the intense premixed combustion zone is getting closer and closer to the plate. At higher values of Φ, the length of the intense premixed combustion zone is exceeding that of the plate.

As Φ is increased, there is increasing contact between the visible flame and the plate. When the flame strikes against the plate, it is forced to spread along it. The flame thins out along the plate which helps to get the flame into contact with secondary air. Thus, the impinging flames are blue in colour at the wall jet regions even at $\Phi = 2.4$. Comparing the open flame with the impinging flames at $\Phi = 2.4$, there is improved air fuel mixing for the impinging flame, as reflected in the colours of the two flames: the open flame

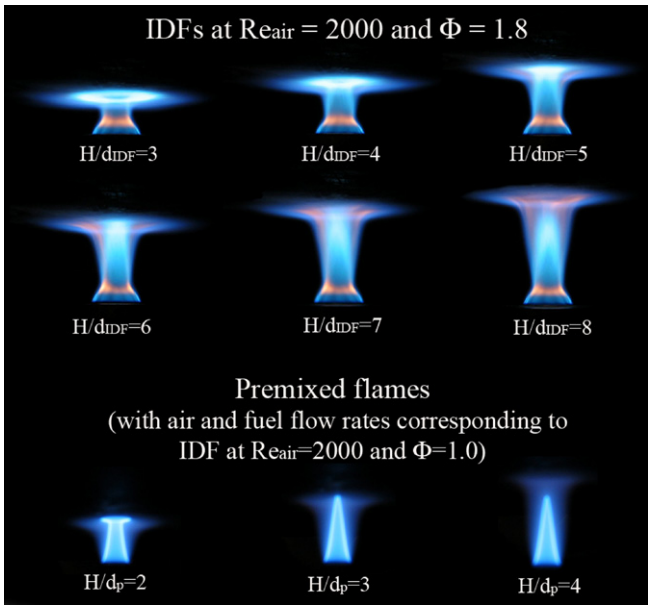

Fig. 3. Effect of nozzle-to-plate distance on impinging IDF and premixed flame.

is mainly yellow while the impinging is almost completely blue.

The upper part of Fig. 3 shows the IDF of $Re_{air} = 2000$ and $\Phi = 1.8$ striking on the plate at H/d_{IDF} of 3–8. The figure shows that at $H/d_{IDF} = 3$, the inner air jet strikes against the centre of the plate. At higher H/d_{IDF}, the premixed reaction zone strikes against the centre of the plate. At $H/d_{IDF} = 8$, the tip of the premixed flame zone fails to reach the center of the plate. Also, as H/d_{IDF} is increased, there is less contact area between the visible flame and the plate. Thus, the nozzle-to-plate distance plays an important role in affecting the heat transfer between the flame and the plate as well as the heat flux distribution on the plate.

The lower part of Fig. 3 shows the corresponding shape of the premixed flame impinging on the plate located at H/d_P of 2, 3 and 4. In this case, the inner cooler air zone is striking against the stagnation point at $H/d_P = 2$; the tip of the reaction zone is striking against the stagnation point at $H/d_P = 3$ and the reaction zone is not reaching the plate at $H/d_P = 4$. Moreover, the visible flame is shorter and has less contact with the impingement plate, compared with an IDF.

3.2. Stagnation point heat flux of impinging IDF

The local heat flux is affected by the upstream combustion conditions. For this reason, the stagnation point heat flux was measured for different nozzle-to-plate distance to identify the effective range of it for further investigation. The results for the IDF for $Re_{air} = 2000$ with different Φ and H/d_{IDF} are shown in Fig. 4. The results obtained for $Re_{air} = 2000$ are similar to those obtained at other values of Re_{air}. The stagnation point heat flux was measured from $H/d_{IDF} = 2$ to $H/d_{IDF} = 16$ at 6 mm interval. With Φ

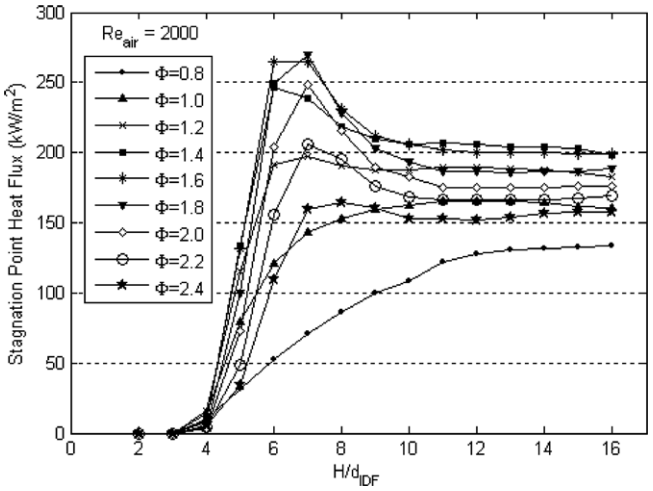

Fig. 4. Stagnation point heat flux of impinging IDF with varied Φ and H/d_{IDF} at $Re_{air} = 2000$.

increasing from 0.8 to 2.4, there is an increasing amount of fuel burn in the flame. There is also an increase in flame length of the corresponding open flame, as shown in Fig. 2.

Fig. 4 shows that the stagnation point profiles can be divided into three groups. The first group corresponds to $\Phi = 0.8$–1.0; the second group for $\Phi = 1.2$–1.8 and the third group for $\Phi > 1.8$. For the first group, the stagnation point heat flux increases as H/d_{IDF} is increased. For the second group, the stagnation point heat flux increases to a peak value and then drops to a lower, steady value as H/d_{IDF} is increased. The peak heat flux is higher at higher Φ, and occurs at lower H/d_{IDF}. For the third group, the stagnation point heat flux also increases to a peak value and then drops to a lower, steady value as H/d_{IDF} is increased. However, the peak heat flux is lower at higher Φ, and occurs at higher H/d_{IDF}. For the last two groups, the peak flux occurs in the range of $H/d_{IDF} = 5$–8 while the steady values occur at about $H/d_{IDF} = 10$. These results are similar to those reported in [13].

The results can be explained with reference to the impinging flames shown in Fig. 2. At $\Phi = 0.8$, the visible flame is not touching the plate at $H/d_{IDF} = 7$. The central air jet draws in the fuel to burn along the periphery of the air jet. The air jet in this case is penetrating through the flame and thus causes a cool core effect. If the plate is at a small distance from the nozzle, the stagnation point will be struck by the cool air, giving a low stagnation point heat flux. However, the influence of the air jet decreases while the influence of the hot gas increases as the nozzle-to-plate distance is increased, which leading to increase stagnation point heat flux as H/d_{IDF} is increased. The stagnation point heat flux at $\Phi = 0.8$ increases to a maximum value at H/d_{IDF} of around 13 and remains rather constant thereafter. The situation is almost the same for $\Phi = 1.0$ except that the stagnation point heat flux is higher than the case of $\Phi = 0.8$ because more fuel is burned, and it increases to a peak value at about $H/d_{IDF} = 11$ and remains rather constant thereafter.

For flames of $\Phi = 1.2$–2.4, the fuel jets are entrained by the air jet and burn to form a bright premixed flame overlapped with a diffusion flame at sufficiently high level of Φ. However, this entrainment weakens at higher level of Φ when the fuel jet velocity becomes higher. The visible flame impinges on and spreads along the plate. Each flame consists of a premixed combustion zone enclosing a cool zone of air. The premixed combustion zone extends in height with an increase in Φ due to the weakened entrainment effect. Thus, the tip of the premixed combustion zone reaches the impingement plate at higher H/d_{IDF} as Φ is increased and finally the cool core starts to impinge on the plate at sufficiently high level of Φ. There are two mechanisms affecting the heat flux at the stagnation point. At lower level of Φ, more fuel is entrained into the premixed combustion zone as Φ is increased, creating higher flame temperature and thus increasing heat flux at the stagnation point. At higher level of Φ, further increase in Φ will reduce fuel entrained due to increased momentum of the fuel jets, causing a cooler premixed flame and decreasing heat flux at the stagnation point. In each case, the heat flux drops at higher H/d_{IDF} because the plate is at a higher position than the position of the tip of the premixed combustion zone. The steady heat flux region at H/d_{IDF} larger than 10 is due to the existence of a fairly constant temperature region beyond the premixed combustion zone of the IDF.

Fig. 4 can also be divided into three zones based on the H/d_{IDF} values. At $H/d_{\mathrm{IDF}} \leqslant 4$, the stagnation point heat flux is very low because it is in contact with the cool air, as reflected in the impinging IDF with $H/d_{\mathrm{IDF}} = 3$ and 4 in Fig. 3. For $H/d_{\mathrm{IDF}} = 5$–10, the heat flux increases subsequently to a peak value and then drops to a steady-state value. For $H/d_{\mathrm{IDF}} > 10$, the stagnation point remains rather steady on further increase to H/d_{IDF} of 16, the largest H/d_{IDF} value being considered in this study. Thus we chose the nozzle-to-plate distance in the range of H/d_{IDF} of 4–10 at $Re_{\mathrm{air}} = 2000$ and $H/d_{\mathrm{IDF}} = 5$–8 at $Re_{\mathrm{air}} = 2500$ and 3000, for $\Phi = 0.8$–1.8 for further investigation on the radial heat flux distribution and heat transfer efficiency.

3.3. Radial heat flux distribution of impinging IDF

Fig. 5 shows the radial heat flux profiles, for the case of $Re_{\mathrm{air}} = 2000$ and $\Phi = 1.8$, at seven different nozzle-to-plate distances corresponding to H/d_{IDF} of 4–10. The corresponding flame images are shown in the upper part of Fig. 3.

The radial profiles for $H/d_{\mathrm{IDF}} = 4$ and 5 has a peak value some distance away from the stagnation point. The heat flux is about 63 kW/m^2 and 118 kW/m^2 at $r/d_{\mathrm{IDF}} = 1$, but increases steeply to the maximum value of 214 kW/m^2 and 206 kW/m^2 at $r/d_{\mathrm{IDF}} = 2$, respectively for $H/d_{\mathrm{IDE}} = 4$ and 5. For this flame, the cool core impinges at the stagnation point while the bright premixed combustion zone impinges at about $r/d_{\mathrm{IDF}} = 2$, and the rest of the flame is forced to spread along the plate. The radial heat flux then drops once the peak value is reached because the flame is

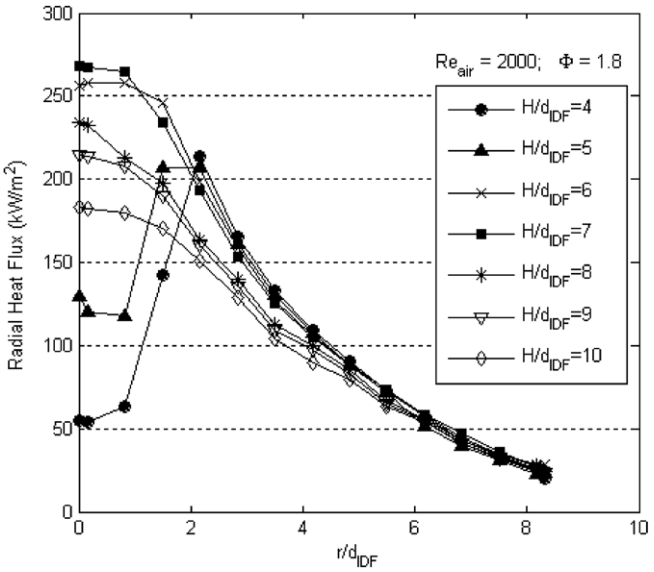

Fig. 5. Radial heat flux of impinging IDF with varied H/d_{IDF} for $Re_{\mathrm{air}} = 2000$ and $\Phi = 1.8$.

spreading radially outwards and becomes cooler and cooler. It is cooled on one side by the plate and on the other side by the ambient air, thus the heat transferred to the plate drops quickly.

When H/d_{IDF} is increased to 6 and 7, the stagnation point heat flux also increases. The peak heat flux occurs close to the stagnation point for $H/d_{\mathrm{IDF}} = 6$, and occurs at the stagnation point for $H/d_{\mathrm{IDF}} = 7$. This is an indication that the bright premixed combustion zone is impinging close to the stagnation at $H/d_{\mathrm{IDF}} = 6$ and impinging at the stagnation point at $H/d_{\mathrm{IDF}} = 7$. The radial profiles are bell shaped in both cases.

For $H/d_{\mathrm{IDF}} = 8$–10, the maximum heat flux also occurs at the stagnation point but the value is much lower than those at $H/d_{\mathrm{IDF}} = 6$ and 7, because the premixed combustion zone is some distance below the impingement plate as the nozzle-to-plate distance is increased, and hence the stagnation point is impinged by the cooler combustion products. The radial heat flux drops rapidly in the radial direction and its local radial heat flux in the wall jet region is even lower than that at $H/d_{\mathrm{IDF}} = 5$. It can be observed that the radial heat flux profile shifts downwards as H/d_{IDF} increases from 8 to 10.

Thus, at H/d_{IDF} of 4 and 5, the nozzle-to-plate distance is too small for full development of the premixed combustion zone. Some unburned air and fuel would be forced to the wall jet region and further react in the wall jet region. When H/d_{IDF} is increased, there is sufficient space for the intense combustion to occur near to the center of the impingement plate. Consequently, local heat flux near the centerline increases and a bell-shaped profile would be obtained. If H/d_{IDF} is further increased, the wall jet region is reduced, indicating that the plate is heated by the combustion products from the reaction zone and the maximum radial heat flux is found at the stagnation point but the

local heat flux is lower because of the cooler flame temperature along the radial profile.

It can be observed that under every considered flame operating conditions, the nozzle-to-plate distance for $H/d_{IDF} = 4$–10 influences the radial heat flux profile mainly in the early wall jet region. At $r/d_{IDF} \geqslant 4$, the seven profiles are close to each other. Fig. 6 shows the radial heat flux distribution at a lower overall equivalence ratio of 1.0. Comparing with Fig. 5, the heat fluxes are lower due to the lower fueling rate. Again, the heat flux distribution in the wall jet region is quite similar for the seven profiles. In this case, the heat flux starts to drop at $H/d_{IDF} = 10$.

Fig. 7 shows the radial heat flux distribution at a higher Re_{air} of 3000 and $\Phi = 1.8$. In this case, due to the increased central air flow rate, the cool core effective is more significant at $H/d_{IDF} = 5$ and occurs even at $H/d_{IDF} = 6$. Comparing with Fig. 5, the heat fluxes are higher due to the higher fueling rate. Again, the heat flux distribution in the wall jet region is quite similar for the four profiles.

A comparison of Figs. 5–7 shows that a change of Re_{air} and Φ will affect the fueling rate and thus the level of heat flux. In the stagnation point region, the heat flux distributions affected by Re_{air} and Φ, as well as the nozzle-to-plate distances. However in the wall jet region, the heat flux distributions affected by Re_{air} and Φ, but only slightly by the nozzle-to-plate distances

3.4. Stagnation point heat flux and radial heat flux distributions of circular premixed impinging flame jet

Fig. 8 shows the stagnation point heat flux for the circular premixed flame jet, measured from $H/d_P = 1$–10 for $\Phi = 1.0$–1.6. The stagnation point heat flux remains very low at low H/d_P and then increases to a peak value as H/d_P is increased. On further increase of H/d_P, the stagnation point heat flux drops to a steady value. The peak stagnation point heat flux occurs at the lowest H/d_P and has the highest value for $\Phi = 1.0$; the peak heat flux drops at higher equivalence ratios and occurs at higher H/d_P. At higher equivalence ratio, the reaction zone of the premixed flame is lengthened due to the higher gas flow rate and hence higher gas velocity. Thus, the tip of the reaction zone strikes the plate at a higher value of H/d_P. Moreover, the flame temperature becomes cooler as the equivalence is increased beyond the stoichiometric value. The patterns in Fig. 8 are significantly different from those in Fig. 4 for the IDF.

The radial heat flux distribution of the premixed flame jet is shown in Fig. 9. The profiles shows that the stagnation point is impinged by cool core gas at $H/d_P = 1.5$, 2

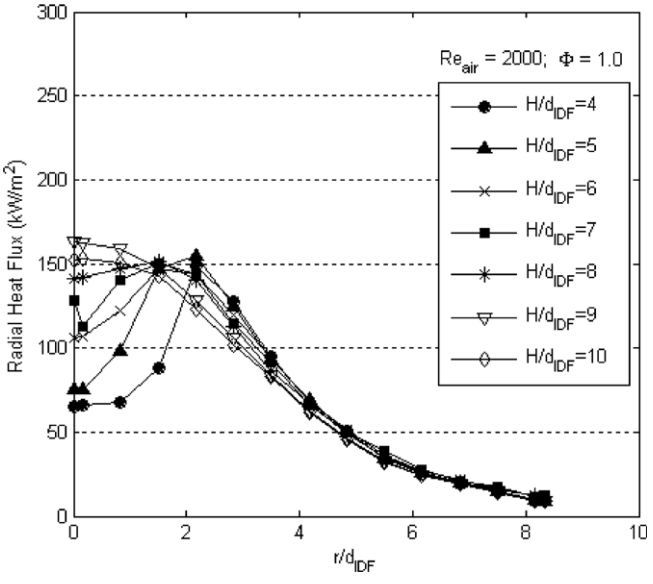

Fig. 6. Radial heat flux of impinging IDF with varied H/d_{IDF} for $Re_{air} = 2000$ and $\Phi = 1.0$.

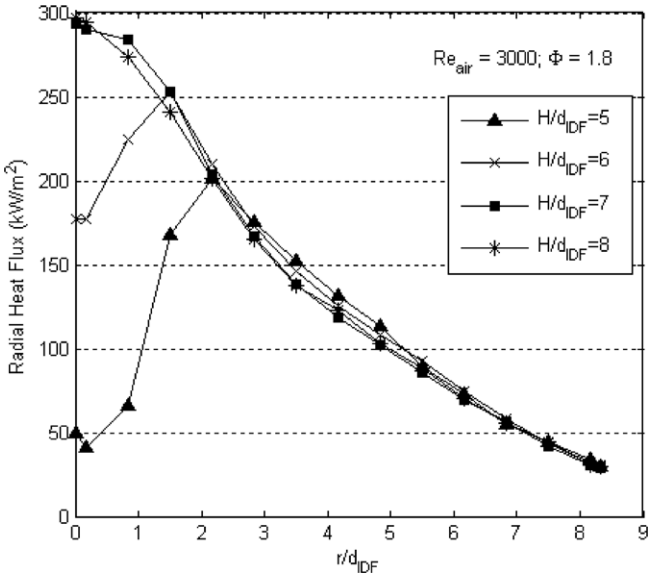

Fig. 7. Radial heat flux of impinging IDF with varied H/d_{IDF} for $Re_{air} = 3000$ and $\Phi = 1.8$.

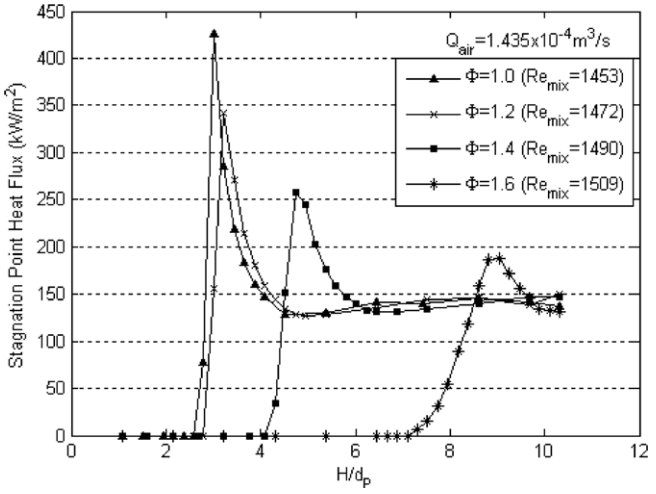

Fig. 8. Stagnation point heat flux of circular premixed impinging flame with varied Φ and H/d_P at constant air flow rate corresponding to IDF with $Re_{air} = 2000$.

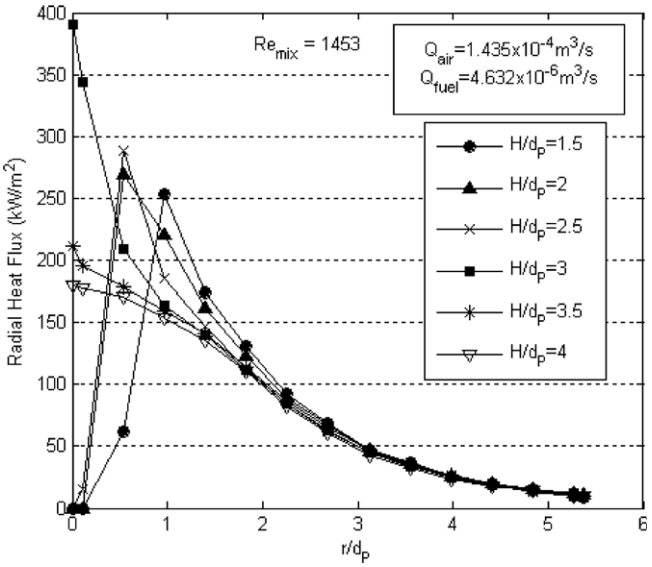

Fig. 9. Radial heat flux of circular premixed impinging flame with varied H/d_P with air flow rate and fuel flow rate corresponding to IDF with $Re_{air} = 2000$ and $\Phi = 1.0$.

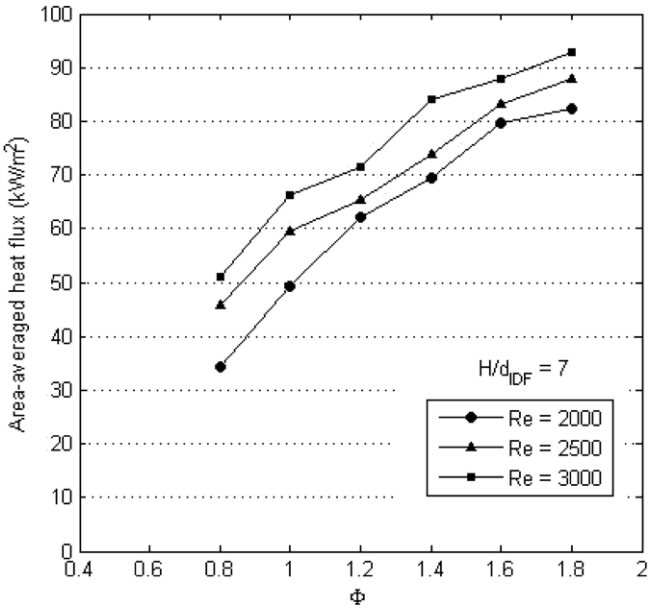

Fig. 10. Variation of area-averaged heat flux with Φ and Re_{air} at $H/d_{IDF} = 7$, impinging IDF.

and 2.5; impinged by the peak of the reaction zone at $H/d_P = 3$; and impinged by the cooler combustion products at $H/d_P = 3.5$ and 4, as reflected in the premixed impinging flames shown in Fig. 3. Again, the profiles are different in the stagnation point region but have little difference in the wall jet region.

The IDF in Fig. 6 and the premixed flame in Fig. 9 have the same air flow rates and fuel flow rates, but their radial heat flux profiles are quite different from each other.

3.5. Area-averaged heat flux and heat transfer efficiency of impinging IDF

The area-averaged heat flux was obtained by considering the heat flux of a circular area within a radial distance of 50 mm from the stagnation point of the flame. Fig. 10 presents the effect of Re_{air} and Φ on the area-averaged heat flux, for $H/d_{IDF} = 7$. Although different radial heat flux profiles are obtained at different heating heights as showed in Figs. 5–7, there is not much difference in the area-averaged heat flux for $H/d_{IDF} = 5$–8 for corresponding values of Re_{air} and Φ. Of all the cases being investigated, the maximum difference is 13.7 kW/m^2, which is found between $H/d_{IDF} = 6$ and 10 at $Re_{air} = 2000$, $\Phi = 1.8$. Hence, the profiles of area-averaged heat flux of other H/d_{IDF} ratios are similar to that shown in Fig. 10.

Fig. 10 shows that in general, the area-averaged heat flux increases with increasing Φ and Re_{air}. An increase in the Re_{air} at fixed Φ means increase in both air and fuel supplies, so that there is an increase in fueling rate and hence area-averaged heat flux. Thus, the profiles shift upwards when Re_{air} is increased. On the other hand, an increase in the Φ at fixed Re_{air} means increase in the fuel flow rate while the air supply remains unchanged. Again, there is an increase in the fueling rate which leads to an increase in the area-averaged heat flux.

The heat transfer efficiency as defined in Eq. (2) is more useful in indicating the effectiveness of energy transferred from the fuel to the impingement plate. Fig. 11 shows the variation of the efficiency with Re_{air} and Φ for $H/d_{IDF} = 5$ and 8. The results are very similar for the two values of H/d_{IDF}. In general, the heat transfer efficiency is the highest for $Re_{air} = 2000$ at $\Phi = 1.0$–1.8. At $\Phi = 0.8$, the heat transfer efficiency at $Re_{air} = 2000$ could drop below those at higher Re_{air}. At $Re_{air} = 2000$, the maximum heat transfer

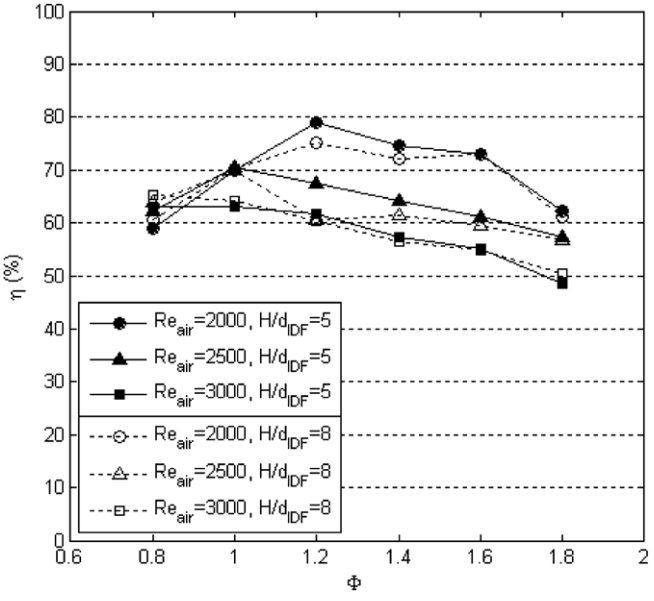

Fig. 11. Variation of heat transfer efficiency with Φ and Re_{air} of the impinging IDF with $H/d_{IDF} = 5$ and $H/d_{IDF} = 8$.

efficiency occurs around $\Phi = 1.2$ and drops on both ends. At $Re_{air} = 2500$, the maximum heat transfer efficiency occurs around $\Phi = 1.0$. At $Re_{air} = 3000$, the maximum heat transfer efficiency occurs at $\Phi = 0.8$. Thus, the maximum heat transfer efficiency shifts towards lower Φ as Re_{air} is increased.

The results are more orderly for $\Phi = 1.2$–1.8. Under this range of overall equivalence ratio, the heat transfer efficiency is always the highest at $Re_{air} = 2000$ and decreases as Re_{air} is increased. There is also a tendency of decreasing heat transfer efficiency with increasing Φ within this range of value. These trends agreed with results in literature for premixed flames [2,3]. One of the major reasons of dropping efficiency with Re_{air} and Φ is due to energy transferred beyond the integration area. As these two parameters are increased in the range of values being investigated, there is an increase in flame length and increase contact with the impingement plate in the wall jet region. Since we have chosen an area for integration, some of the energy transferred beyond the chosen area will not be taken into account. As Re_{air} and Φ are increased, there is increasing amount of energy transferred beyond the integrated area which results in decreasing efficiency.

3.6. Comparison of area-average heat flux and heat transfer efficiency of impinging IDF and premixed impinging flame

The effects of nozzle-to-plate distance on the area-averaged heat flux and the heat transfer efficiency of the premixed flame are compared in Fig. 12. Since the premixed flame has heat released at smaller H than the IDF, the area-averaged heat flux and the heat transfer efficiency are compared at the heights corresponding to their own range of intense combustion region. The heights chosen for the premixed flame are $H = 14$–37.2 mm (corresponding to $H/d_P = 1.5$–4); and that for the IDF are $H = 24$–60 mm (corresponding to $H/d_{IDF} = 4$–10). Fig. 12 show the area-averaged heat flux and the heat transfer efficiency of the two flames operating at $\Phi = 1.0$ and $\Phi = 1.2$ under the same air flow rate of $Q_{air} = 1.435 \times 10^{-4}$ m^3/s, corresponding to $Re_{air} = 2000$ in the IDF.

The figures show that, for each type of flame, there is certain variation in the area-averaged heat flux and the heat transfer efficiency in the range of nozzle-to-plate distance being investigated. At $\Phi = 1.0$, the premixed flame have higher level of area-averaged heat flux and heat transfer efficiency than the IDF. For the premixed flame, the highest heat transfer efficiency of 78.1% is obtained at $H = 8.6$ mm ($H/d = 2$), in which case H is slightly lower than the tip of the reaction zone. The result agrees with the finding of Hou and Ko [10]. The lowest heat transfer efficiency of the premixed flame is 66.3%. Thus there is a difference of 11.8% over a nozzle-to-plate distance of 23.2 mm. For the IDF, the maximum heat transfer efficiency is only 72.1% at H/d_{IDF} of 6 while the lowest one is 64.7%. Thus there is a difference of 7.4% over a nozzle-to-plate distance of 36 mm.

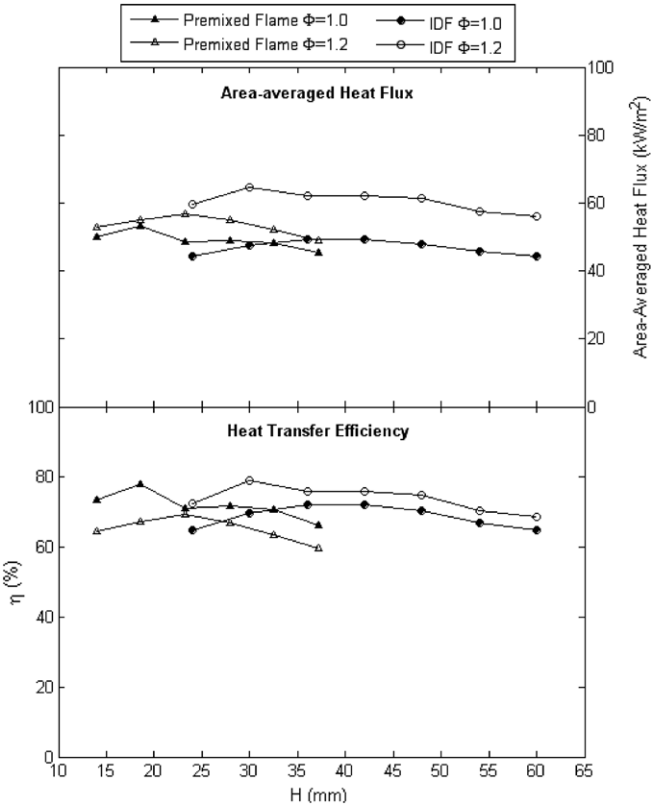

Fig. 12. Comparisons of area-averaged heat flux and heat transfer efficiency, for the impinging IDF and premixed flame under identical volume flow rates of air and fuel: $Q_{air} = 1.44 \times 10^{-4}$ m^3/s ($Re_{air} = 2000$); $Q_{fuel} = 4.63 \times 10^{-6}$ m^3/s ($\Phi = 1.0$) and $Q_{fuel} = 5.56 \times 10^{-6}$ m^3/s ($\Phi = 1.2$).

When Φ is increased to 1.2, the area-averaged heat flux of both flame increases. For the same increase in fuelling rate, the area-averaged heat flux has increased by an average of 13.7 kW/m^2 for the IDF, but for the premixed flame, the average increase is only 4.3 kW/m^2. This results in an increase in the heat transfer efficiency of the IDF and a reduction in the premixed flame, compared with their corresponding values at $\Phi = 1.0$. The maximum heat transfer efficiency of the IDF is 79.0% at H/d_{IDF} of 5 while for the premixed flame, the maximum heat transfer efficiency drops to 69.2% at H/d_P of 2.5.

An observation of the flames shows that the IDF at $\Phi = 1.0$ is in fact fuel lean while at $\Phi = 1.2$, the flame gets closer to stoichiometric. For the premixed flame, it is stoichiometric at $\Phi = 1.0$ but becomes fuel rich at $\Phi = 1.2$. Therefore there is an increase in the heat transfer efficiency of the IDF but a decrease for the premixed flame when the Φ of the flame was increased from 1.0 to 1.2. Fig. 12 shows that the heat transfer efficiency of the IDF at $\Phi = 1.2$ is even higher than that of the premixed flame at $\Phi = 1.0$ over the range of nozzle-to-plate distance investigated.

Thus, for a premixed flame, the heat transfer efficiency is more sensitive to the nozzle-to-plate distance than the IDF. The IDF could have comparable or even higher heat transfer efficiency than a premixed flame over a large range of nozzle-to-plate distance.

4. Conclusions

Experimental studies were performed in which the heat transfer characteristics and heat transfer efficiency of an IDF burning LPG were investigated and compared with those of a premixed flame. The stagnation point heat flux were measured to determine the most vigorous combustible region over a range of overall equivalence ratio in the IDF; and the local radial heat flux were measured to determine the area-averaged heat flux and the heat transfer efficiency.

Flame images of the open flame and the impinging flames were used to explain the trends of the heat flux data. The flame images show that an increase in Re_{air} and Φ will increase the fueling rate and hence the flame length. This will affect the contact between the flame and the plate, as well as the intensity of heat flux.

For the IDF, the area-averaged heat flux increased with either Re_{air} or Φ, since both imply an increase in the fueling rate. However, there is little variation of the area-average heat flux with H/d_{IDF} for the range of H/d_{IDF} from 4 to 10. The heat transfer efficiency, for the range of Re_{air} and Φ investigated, has a peak value at $Re_{air} = 2000$ and $\Phi = 1.2$. At higher Re_{air} and at higher Φ, the heat transfer efficiency decreases. One of the main reasons of the drop in heat transfer efficiency is due to the heat escaped beyond the integration area used for the evaluation of the heat transfer efficiency.

A comparison of the results with a premixed flame shows that the stagnation point heat flux and the radial heat flux profiles are quite different. The premixed flame has intense combustion in a shorter flame length while the IDF has intense combustion over longer flame length. The heat transfer efficiency of the premixed flame has a peak value at $\Phi = 1.0$ at $H/d_P = 2$ and decreases at higher Φ and higher or lower H/d_P. The IDF could have comparable or even higher heat transfer efficiency than a premixed flame over a large range of nozzle-to-plate distance.

Acknowledgements

The authors thank The Hong Kong Polytechnic University and the Research Grants Council of the Hong Kong SAR in supporting this study (Project No.: PolyU 5142/05E).

References

[1] S. Chander, A. Ray, Flame impingement heat transfer: a review, Energy Conver. Manage. 46 (2005) 2803–2837.

[2] L.L. Dong, C.S. Cheung, C.W. Leung, Heat transfer from an impinging premixed butane/air slot flame jet, Int. J. Heat Mass Transfer 45 (2002) 979–992.

[3] L.C. Kwok, C.W. Leung, C.S. Cheung, Heat transfer characteristics of slot and round premixed impinging flame jets, Exp. Heat Transfer 16 (2003) 111–137.

[4] X.Q. Huang, C.W. Leung, C.K. Chan, S.D. Probert, Thermal characteristics of a premixed impinging circular laminar-flame jet with induced swirl, Appl. Energy 83 (2006) 211–401.

[5] S.G. Tuttle, B.W. Webb, M.Q. McQuay, Convective heat transfer from a partially premixed impinging flame jet. Part I: time-average results, Int. J. Heat Mass Transfer 48 (2005) 1236–1251.

[6] Z. Zhao, T.T. Wong, C.W. Leung, Impinging premixed butane/air circular laminar flame jet—influence of impingement plate on heat transfer characteristics, Int. J. Heat Mass Transfer 47 (2004) 5021–5031.

[7] L.L. Dong, C.W. Leung, C.S. Cheung, Heat transfer of a row of three butane/air flame jets impinging on a flat plate, Int. J. Heat Mass Transfer 46 (2003) 113–125.

[8] L.L. Dong, C.W. Leung, C.S. Cheung, Heat transfer and wall pressure characteristics of a twin premixed butane/air flame jets, Int. J. Heat Mass Transfer 47 (2004) 489–500.

[9] L.C. Kwok, C.W. Leung, C.S. Cheung, Heat transfer characteristics of an array of impinging pre-mixed slot flame jets, Int. J. Heat Mass Transfer 48 (2005) 1727–1738.

[10] S.S. Hou, Y.C. Ko, Effects of heating height on flame appearance, temperature field and efficiency of an impinging laminar jet flame, Energy Conv. Manage. 45 (2004) 1583–1595.

[11] K. Mizuno, R. Mital, R. Viskanta, An experimental study of premixed flame impingement heat transfer, Proc. ASME Heat Transfer Div. 4 (1996) 245–252.

[12] C.E. Baukal, B. Gebhart, Heat transfer from oxygen-enhanced/natural gas flames impinging normal to a plane surface, Exp. Thermal Fluid Sci. 16 (1998) 247–259.

[13] L.K. Sze, C.S. Cheung, C.W. Leung, Temperature distribution and heat transfer characteristics of an inverse diffusion flame with circumferentially, Int. J. Heat Mass Transfer 47 (2004) 3119–3129.

[14] K.T. Wu, R.H. Essenhigh, Mapping and structure of inverse diffusion flames of methane, in: Proceedings of the 20th Symposium (International) on Combustion, 1984, pp. 1925–1932.

[15] G.W. Sidebotham, I. Glassman, Flame temperature, fuel Structure, and fuel concentration effects on soot formation in inverse diffusion flames, Combust. Flame 90 (1992) 269–283.

[16] A. Sobiesiak, J.C. Wentzell, Chatacteristics and structure of inverse flames of natural gas, Proc. Combust. Inst. 30 (2005) 743–749.

[17] T. Takagi, Z. Xu, M. Komiyama, Preferential diffusion effects on the temperature in usual and inverse diffusion flames, Combust. Flame 106 (1996) 252–260.

[18] C.R. Kaplan, K. Kailasanath, Flow-field effects on soot formation in normal and inverse methane—air diffusion flames, Combust. Flame 124 (2000) 275–294.

[19] L.K. Sze, C.S. Cheung, C.W. Leung, Appearance, temperature, and NO_X emission of two inverse diffusion flames with different port design, Combust. Flame 144 (2006) 237–248.

[20] S.J. Kline, F.A. McClintock, Describing uncertainties in single-sample experiments of temperature in flames, Mech. Eng. 75 (1953) 3–8.

[21] M. Mahmood, Heat Transfer from Swirling Impinging Jets, Ph.D. Thesis, Cranfield Institute of Technology, 1980.